Facile Synthesis of Ni-MgO/CNT Nanocomposite for Hydrogen Evolution Reaction

P. Mohana , M. Isacfranklin , R. Yuvakkumar * , G. Ravi , L. Kungumadevi , S. Arunmetha , J.H. Han , S. I. Hong *

Posted Date: 26 December 2023

doi: 10.20944/preprints202312.1992.v1

Keywords: Water splitting; hydrogen evolution reaction; chemical vapour deposition; overpotential and hydrogen production.

Article

Facile Synthesis of Ni-MgO/CNT Nanocomposite for Hydrogen Evolution Reaction

P. Mohana [1], M. Isacfranklin [1], R. Yuvakkumar [1,*], G. Ravi [1,2], L. Kungumadevi [3], S. Arunmetha [4], J.H. Han [5] and S.I. Hong [5,*]

[1] Department of Physics, Alagappa University, Karaikudi 630 003, Tamil Nadu, India
[2] Department of Physics, Chandigarh University, Mohali 140 413, Punjab, India
[3] Department of Physics, Mother Terasa Women's University, Kodaikanal, India
[4] Department of Electronics and communication Engineering, Koneru Lakshmaiah Education Foundation, Guntur, Andhra Pradesh 522 502, India
[5] Department of Materials Science and Engineering, Chungnam National University, Daejeon, 34134, Republic of Korea
* Correspondence: R Y: yuvakkumarr@alagappauniversity.ac.in; SIH: sihong@cnu.ac.kr

Abstract: In this study, the pristine MgO, MgO/CNT and Ni-MgO/CNT nanocomposites were processed by the impregnation and chemical vapour deposition methods and analyzed for hydrogen evolution (HER) via electrochemical water splitting process. Furthermore, effect of nickel on the deposited carbon was systematically elaborated in this study. The highly conductive carbon nanotubes (CNTs) deposited on the metal surface of the Ni-MgO nanocomposite heterostructure provides the robust stability and superior electrocatalytic activity. The optimized Ni-MgO/CNT nanocomposite exhibited hierarchical helical-shaped carbon nanotubes adorned on the surface of the Ni-MgO flakes, forming a hybrid metal-carbon network structure. The HER catalytic reaction was carried out in 1M alkaline KOH electrolyte, and the optimized Ni-MgO/CNT nanocomposite achieves the low 117 mV overpotential value (η) at the 10 mA cm^{-2} and needs low 116 mV/dec Tafel value denoted Volmer-Heyrovsky pathway. Also, high electrochemical active surface area (ECSA) value of Ni-MgO/CNT nanocomposite acquires 515 cm^2, which is favorable for the generation of abundant electro-active species and the prepared electrocatalyst durability was also performed by chronoamperometry test for prolonged duration of 20 h at 10 mA cm^{-2} and exhibits the good stability with 72% retention. Hence, obtained results demonstrated that the optimized Ni-MgO/CNT nanocomposite is highly active and cost-effective electrocatalyst towards hydrogen energy production.

Keywords: Water splitting; hydrogen evolution reaction; chemical vapour deposition; overpotential and hydrogen production

1. Introduction

In an ever-expanding global landscape, the imperative for energy harvesting becomes increasingly vital to minimize the energy loss and gather many different forms of energies to meet the escalating demand for energy driven by surging global population. This necessity is further featured by the imperative to sustain the socio-economic progress, enhance the well-being, and safeguard the public health. Simultaneously, the exponential growth in population has become a catalyst for a spectrum of environmental challenges, notably the alarming rise in greenhouse gas emissions. Consequently, amidst this complex scenario, the pressing need arises for a transition towards renewable energy including solar, wind power, biomass, and biogas, which may offer a sustainable alternative to fulfill the energy requirements of the burgeoning population while mitigating the adverse impacts associated with the depletion of finite fossil resources. This shift towards the renewable energy not only addresses the immediate energy needs but also aligns with the imperative of fostering a more sustainable and to contribute a more environmentally conscious energy landscape [1]. In the pursuit of establishing a clean and sustainable energy production paradigm, molecular hydrogen (H_2) has garnered recognition as a carbon-free alternative. Renowned

for exceptional gravimetric energy density, reaching approximately 282 KJ mol^{-1} and hydrogen stands out as a highly efficient and eco-friendly option. This characteristic makes it an appealing choice in the quest for sustainable energy solutions, offering the potential to significantly reduce carbon emissions [2]. Industrial hydrogen production, so far, has predominantly relied on the conventional steam-methane reforming method. A notable drawback of this approach, however, is the inherent generation of hazardous carbon dioxide (CO_2) emissions during the reaction process. This poses a significant environmental concern as it contributes to the ever-increasing issue of greenhouse gas emissions, underscoring the pressing need for alternative and sustainable methods in hydrogen production to mitigate these adverse environmental impacts [3]. Over the past few decades, electrocatalytic water splitting has been adopted by researchers as promising and effective technique for pure hydrogen production [4–7]. Electrocatalysis of water primarily have two half redox reactions: anodic oxygen evolution (OER) with four electron step transfer and cathodic hydrogen evolution reaction (HER) with two electron step transfer [5]. The efficient hydrogen evolution reaction was mainly comprised two reaction mechanism named as Volmer-Heyrovsky and Volmer-Tafel mechanism. In those two steps, hydrogen generation proceeded depending on the process of adsorption (Volmer), desorption and recombination (Heyrovsky and Tafel) process of the adsorbed hydrogen (H*) and hydroxide ions (OH^-) which plays vital role for the H_2 generation and high HER catalytic performance. To this date, noble catalysts such as Pt/C or Ru/IrO_2 based materials exhibited outstanding electrocatalytic performance towards overall electrochemical water splitting [6–10]. Consequently, the expensive costs and instability of those worthy candidates severely limit the growth of industrial applications. Therefore, switching to efficient non-noble catalysts at a lower cost with enhanced electrocatalytic performance is highly advisable to provide sustainable alternative energy [10,11]. Recently, transition metal based electrocatalysts like oxides/hydroxides, sulphides, carbides, nitrides and phosphides etc. are widely explored in many energy conversion and storage applications owing to their high stability, affordability, earth rich nature [12]. Among many metal-oxides based electrocatalysts, magnesium oxide (MgO) has attracted great interest due to their large surface sites, lattice defects, ion vacancies that can promote the surface chemical kinetics and its catalytic behavior [13,14].

The single metal oxides, however, are known to possess the lack of stability, low conductivity and inferior catalytic activity which may obstructs the improvement of catalytic activity at the large scale level. On the other hand, carbon materials can be used as potential additives for the formation of nanocomposites with the improved catalytic conductivity and active site dispersibility [15]. Carbon nanotubes have attracted the significant attention in the development of advanced sustainable energy storage applications. The formation of nanocomposites of metal oxides and CNTs facilitates the access to metal carbon surfaces for better charge storage activities of high electrolyte ions and amplifies specific material surface area [16]. Ni has been recognized as an effective element to form the metal-metal oxide carbon lattice structure due to the high redox active sites and known to enhance the electrical conductivity and stability [17]. Wei Liu et al [18] achieved low 70 mV overpotential values at 10 mA cm^{-2} in alkaline medium using Ni-Mg-La for HER studies. Darband et al [19] synthesized Ni-CNT nanocomposite via electrodeposition method and achieve low overpotential value of 82, 116 and 207 mV at 10, 20 and 100 mA cm^{-2}.

In this study, various synthesis methods were explored, including the hydrothermal processes, microwave-assisted electrodeposition, chemical vapor deposition, sol-gel techniques, etc and developed the three-dimensional hierarchical nanostructures comprising metal-carbon nanocomposites with the enhanced electrocatalytic activity [20–24]. We also specifically focused on elucidating the heterogeneous electrocatalytic action of the composite structure in facilitating the hydrogen evolution reaction.

Preprints (www.preprints.org) | NOT PEER-REVIEWED | Posted: 26 December 2023 doi:10.20944/preprints202312.1992.v1

2. Materials and Methods

2.1. Materials

Magnesium oxide light LR (MgO) was acquired from S.D. Fine Chem. Ltd., while nickel(II) nitrate hexahydrate ($Ni(NO_3)_2{\cdot}6H_2O$) was obtained from Sigma Aldrich. High-purity nitrogen (99.999%), hydrogen (99.99%), and acetylene (99.9999%) were sourced from Success Trader for use in our experimental procedures.

2.2. Synthesis procedure

MgO (0.7 g) powders were placed in CVD under inert gas atmosphere (N_2) for 1 h 40 min to reach 500°C and, then, H_2 +N_2 gases were passed to reduce the catalyst with the gradual increase of temperature from 500°C to 800°C during the period of 1 hour. After the temperature was reached 800°C, precursor gas (C_2H_2) was introduced to induce slow cooling for 30 minutes. Meanwhile, the solution of 0.2 g $Ni(NO_3)_2{\cdot}6H_2O$ dissolved in 20 ml distilled water (stirred for 30 min) was prepared. As 0.2 g of magnesium oxide (MgO) was completely dissolved in the mixed solution after approximately 1 h, the colour of solution gradually changed from pale white to pale green. The prepared material was filtered using the distilled water, acetone and methanol. Ni-MgO powder was placed in CVD under inert gas atmosphere (N_2) for 1 hour 40 minutes until the temperature reached 500°C. Then, H_2+N_2 gases were supplied to reduce catalyst and promote carbon nanotubes growth on it for 1 h at 500°C. The temperature was then increased from 500 to 800°C for 1h. After the temperature reaches 800°C, precursor gas (C_2H_2) was introduced for 30 min and subsequently it was slowly cooled. The preparation of Ni-MgO/CNT nanocomposite is shown in Scheme 1.

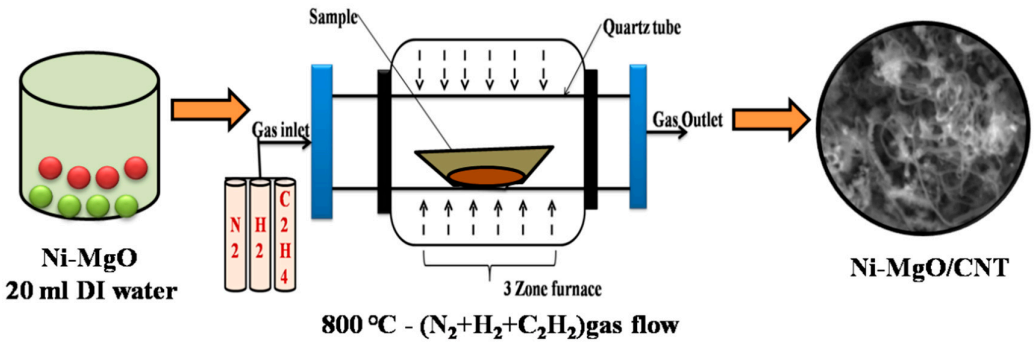

Scheme 1. Ni-MgO/CNT nanocomposite preparation.

2.3. Characterizations

The electrochemical study was conducted employing Bio-logic SP-150 workstation. Slurry of working substance was carefully produced employing MgO, MgO/CNT and Ni-MgO/CNT catalyst, activated carbon, and polyvinylidene fluoride (PVDF) in 80:10:10 ratios, respectively. Manual mixing was performed in few drops of N-methyl pyrrolidinone (NMP). Ni substrate was subjected to pre-cleaning with 1 M HCl in 100 mL of de-ionized (DI) water employing ultrasonication for 30 minutes, effectively removing the NiOx surface layer. For electrochemical studies, the catalyst-coated Ni foam (1×1 cm^2) served as the working electrode, Pt wire was used as the counter, and Ag/AgCl electrode functioned as the reference electrode in 3-electrode system, specifically for HER applications. 1 M KOH solution was used as an alkaline electrolyte. All potential was referenced to reversible hydrogen electrode (RHE) using Nernst equation. To probe dynamics of the electrochemical reaction process, electrochemical impedance spectroscopy (EIS), additionally with chronoamperometry study was carried out with 10 mA cm^{-2} to further evaluate the electrochemical performance. The structural and phase purity was studied employing High-Temperature Powder X-ray Diffractometer (HT-XRD) equipped with HTK 1200N – Bruker D8 Advance. Additionally, small changes in the structural

 doi:10.20944/preprints202312.1992.v1

morphology and disorder of carbon nanomaterials were detected using Micro-Laser Raman instruments (Seiki, Japan). Furthermore, the morphologies of the sample was examined through the utilization of a CAREL ZEISS EVO 18 scanning electron microscope and a JEOL-2100+ High-Resolution Transmission Electron Microscope. The composition and chemical state of Ni-MgO/CNT was examined employing a PHI-VERSAPROBE III – X-ray Photoelectron Spectroscopy. Electrochemical study was conducted employing a Biologic SP-150 instrument to investigate the electrochemical properties of the system under study.

3. Results and Discussion

3.1. Phases and chemical structure analysis

In order to explore the phase stabilities and nanostructures of MgO, MgO/CNT and Ni-MgO/CNT, constituent phases were explored using the X-ray diffraction (XRD). Figure 1 exhibits the XRD peaks from MgO (dark blue), MgO/CNT (green) and Ni-MgO/CNT (pink). All the characteristic peaks shown in the XRD pattern of MgO (dark blue) are related with the peaks from (111), (200), (220) and (222) crystalline planes of MgO (standard JCPDS card no 75-1525) with the cubic crystal under Fm-3m space group as explored in the earlier reports [25]. The high intensity and sharp peaks of MgO/CNT demonstrated the prepared product good crystallinity. Also, diffraction peak at 25° to 26° indicates the presence of carbon peak due to hexagonal graphite structure. No impurities or extra diffraction peaks founded with the addition of CNT, which confirmed the phase purity of the material formations. The comparison of the peaks from Ni-MgO/CNT to those from MgO/CNT revealed no major differences except the broad and low intensity peak at $2\theta = 44.2°$ in Ni-MgO/CNT. No clear crystalline peaks observed from (111), (200) and (220) peaks from crystalline Ni [26]. The broad and low intense diffraction peak centered at around 44~45° are known to belong to the amorphous Ni (JCPDS card no 87-0712) [26,27]. It is interesting to note that no sharp peaks from Ni were observed in Ni-MgO/CNT. The formation of amorphous Ni using nickel nitrate hexa hydrate ($Ni(NO_3)_2{\cdot}6H_2O$) by liquid-phase chemical reduction approach has been reported previously [27].

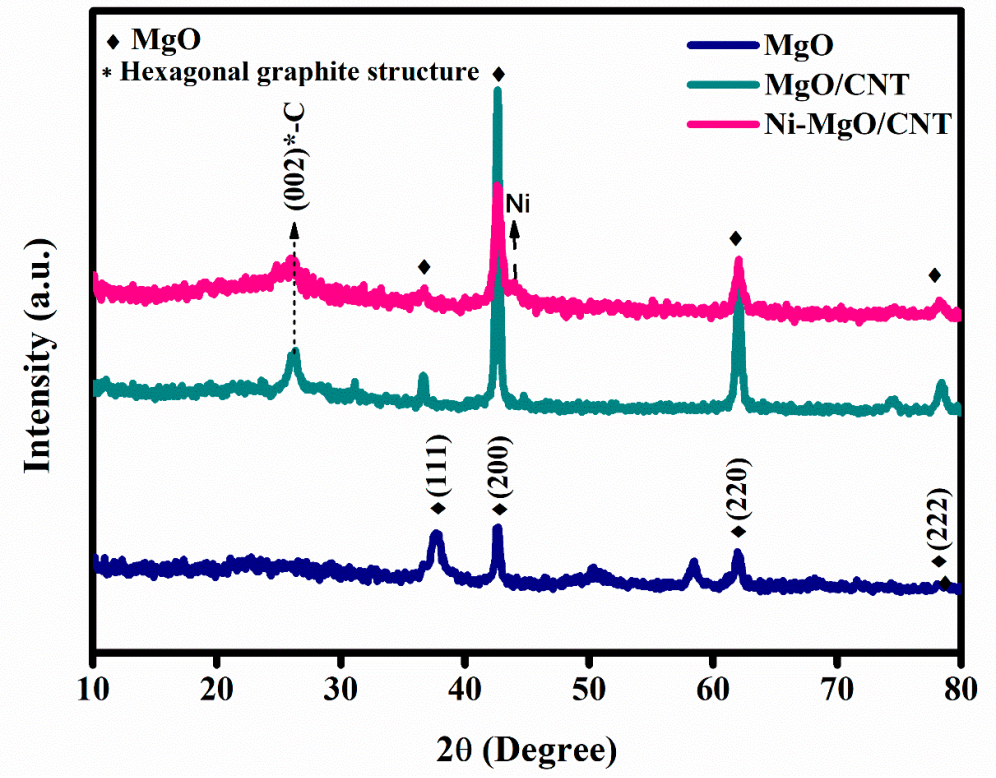

Figure 1. XRD analysis (a) MgO, (b) MgO/CNT and (c) Ni-MgO/CNT.

Preprints (www.preprints.org) | NOT PEER-REVIEWED | Posted: 26 December 2023 doi:10.20944/preprints202312.1992.v1

Figure 2 demonstrates the difference of characteristic chemical structures of as-prepared pristine MgO, MgO/CNT and Ni-MgO/CNT samples revealed by Raman studies. For pristine MgO (dark blue), a small peak observed at 442 cm^{-1} is linked with the presence of Mg and peak located at 3656 cm^{-1} indicates vibrational broadening of –OH group. The spectra in MgO/CNT (green) and Ni-MgO/CNT (pink) in Figure 2 demonstrates the presence of two pronounced bands at 1333 (D-band) and 1591 cm^{-1} (G-band). The D-band is known to reveal the defects, or lattice distortions of carbon atoms, whereas the G-band is correlated with graphite E_{2g} and/or is brought about by sp^2-bonded carbon atoms. The crystallinity of graphite or CNT is supported by G band in Figure 2. The I_D/I_G in Figure 2 was estimated with values of 2.11 and 0.97 for Ni-MgO/CNT and MgO/CNT electrocatalyst respectively. Transient metals such as Fe, Co, and Ni are commonly used as the catalyst for the CNT synthesis [28–32]. The G-band to D-band relative intensity ratio is greater in Ni-MgO/CNT, indicating more defects in the synthesized Ni-MgO/CNT compared to those in MgO/CNT. The more defects might be introduced during the rapid growth of CNT promoted by the catalysis reaction of Ni. Small peaks situated at 2676 and 2933 cm^{-1} were revealed the second order of 2D and G' band. A small peak observed at 2933 cm^{-1} is known to be a characteristic of the presence of CNTs. Here, the presence of G' band supports the higher fraction of CNTs in Ni-MgO/CNT than in MgO/CNT (green), although more defects were introduced in CNT of Ni-MgO/CNT [28–32] because of its faster growth facilitated by the catalytic function of Ni.

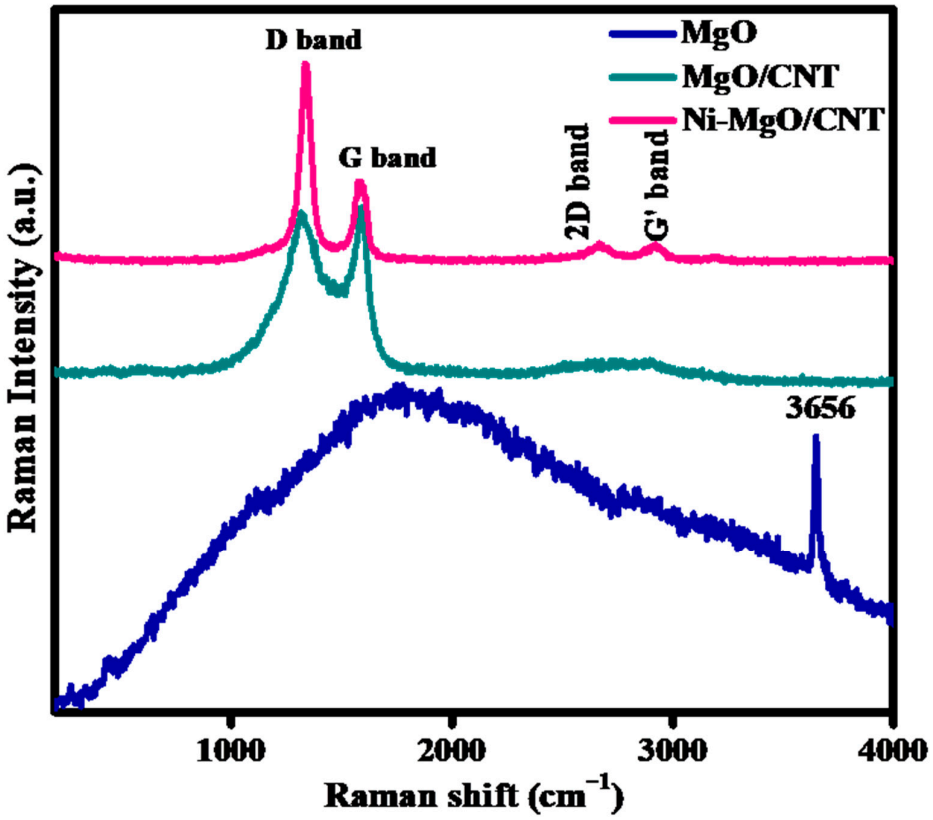

Figure 2. Raman spectra (a) MgO, (b) MgO/CNT and (c) Ni-MgO/CNT.

3.2. Microstructural/Nanostructural analysis

Figure 3 shows surface morphologies of as synthesized MgO (a-c), MgO/CNT (d-f) and Ni-MgO/CNT (g-i) electrode materials observed using the scanning electron microscope (SEM). Figure 3(a) shows the plate-like fuzzy appearance for MgO sample [33–35]. The high magnification image in Figure 3(b) and Figure 3(c) clearly exhibits the plate-shaped MgO crystals on the surface. The (100) plane of MgO is suggested to be the most stable due to its low surface energy [33], and (110) plane is

 doi:10.20944/preprints202312.1992.v1

therefore naturally exposed after cleavage, and it is the most favorably exposed surface generated also by wet chemical methods as shown in the present study. The plate-shaped crystals are likely MgO crystals [33]. Figure 3(d-f) depicts the morphology of CNTs grown on MgO using acetylene (C_2H_4) as a carbon precursor at 800°C for 20 minutes of gas flow. The long and thin curly tube-shaped CNTs are found to be formed over MgO synthesized from acetylene (C_2H_4) precursor at 800°C for 20 minutes gas flow. The approximate thickness and the length of CNTs formed on the surface of MgO catalysts were observed to be about ~100 nm and few micro-meters, respectively. Figure 3(g-i) displays the well-aligned helical-shaped CNTs on flake-like structure of Ni-MgO, which clearly revealed the formation of a fair amount of curly CNTs on the surface induced by the catalytic effect of Ni on the substrate surface. The abundance of CNTs in Ni-MgO/CNT (Figure 3(h), 3(i)) compared to those in MgO/CNT (Figure 3(e), 3(f))supports the faster growth facilitated by the catalytic action. Furthermore, CNTs diameter could be decreased by adding the small amount of Ni content [35].

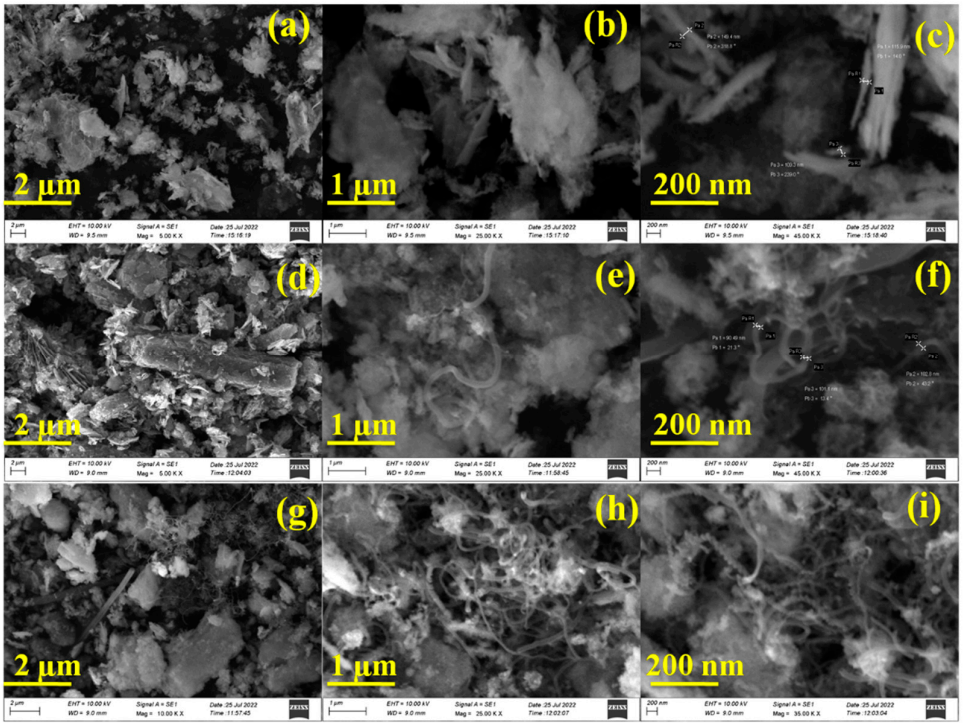

Figure 3. FE-SEM studies (a-c) MgO, (d-f) MgO/CNT and (g-i) Ni-MgO/CNT.

The nanostructure of the synthesized Ni-MgO/CNT nanocomposite was examined using the transmission electron microscopy (TEM) study and its nanostructural details are illustrated in Figure 4(a-h). High magnification TEM images presented in Figure 4(a-c) vividly exhibit the morphology of nanoflakes encapsulated by conductive carbon nanotubes (CNTs) with the average diameter ranged 15-25 nm. These observations align well with the findings from scanning electron microscopy (SEM) studies. Furthermore, Figure 4 (f,g) distinctly revealed lattice fringes corresponding to MgO (111) and (200) planes, with interlayer distances of 0.29 and 0.32 nm, respectively, consistent with the results obtained from XRD analyses. The nanostructure of the Ni-MgO/CNT nanocomposite is further validated by selected area electron diffraction (SAED) presented in Figure 4 (h), highlighting lattice planes (111), (200), (220), and (222), corresponding well with the XRD results [36–39].

Preprints (www.preprints.org) | NOT PEER-REVIEWED | Posted: 26 December 2023 doi:10.20944/preprints202312.1992.v1

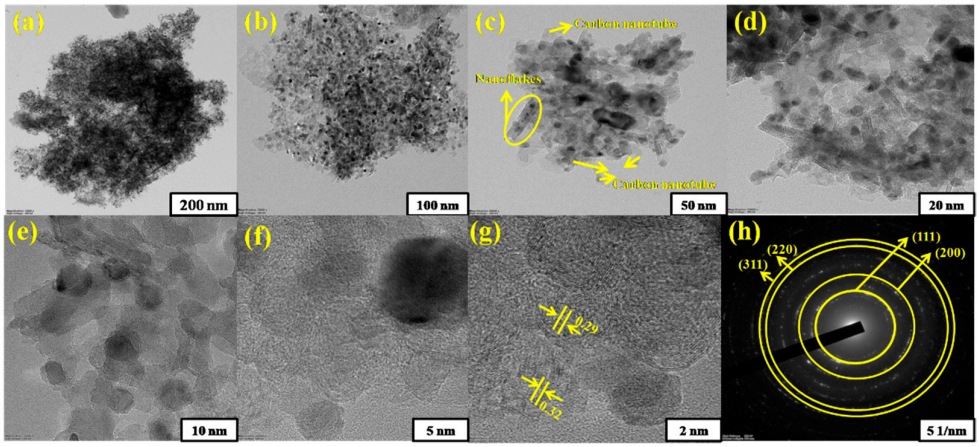

Figure 4. TEM studies (a-c) Ni-MgO/CNT, (d,e) lattice fringes of Ni-MgO/CNT and (f) SAED pattern of Ni-MgO/CNT.

The surface elemental composition and chemical and binding energy were analyzed by X-ray photoelectron spectra (XPS). The successful formation of Ni-MgO/CNT nanocomposites with the constituent elements of Ni, Mg, O and C is confirmed by peaks from these constituent elements as exhibited in Figure 5(a). The core broad spectrum of Ni 2p at 855 eV can be assigned to Ni $2p_{3/2}$ and their satellite peaks observed at 860.3 eV denotes the abundant presence of Ni^{2+} oxidation state. Additionally, a peak at 871 eV can be assigned to Ni $2p_{1/2}$ in Figure 5(b) [40]. The typical peaks of Mg 2s located in the binding energy at 88.7, 90.0, 91.3 eV can be attributed to those from the metallic Mg, the surface MgO layer and the chemisorbed surface compounds of Mg with the carbon and oxygen such as MgOH and MgCO as depicted in the Figure 5(c) [41]. The O1s spectra of oxygen positioned at 527.1, 531 and 532.9 eV in Fig. 5(d) corresponds to the oxygen functional groups of C=O, C-O-C/C-O-H and O=C-O observed for Ni-MgO/CNT which is appeared in the Figure 5(d) [42]. The C1s spectra at 284, 284.6, 285.1 and 286.1 eV in Figure 5(e) of the prepared electrocatalyst represent the peaks associated with the C-C, C=O, C-O and C-N [43].

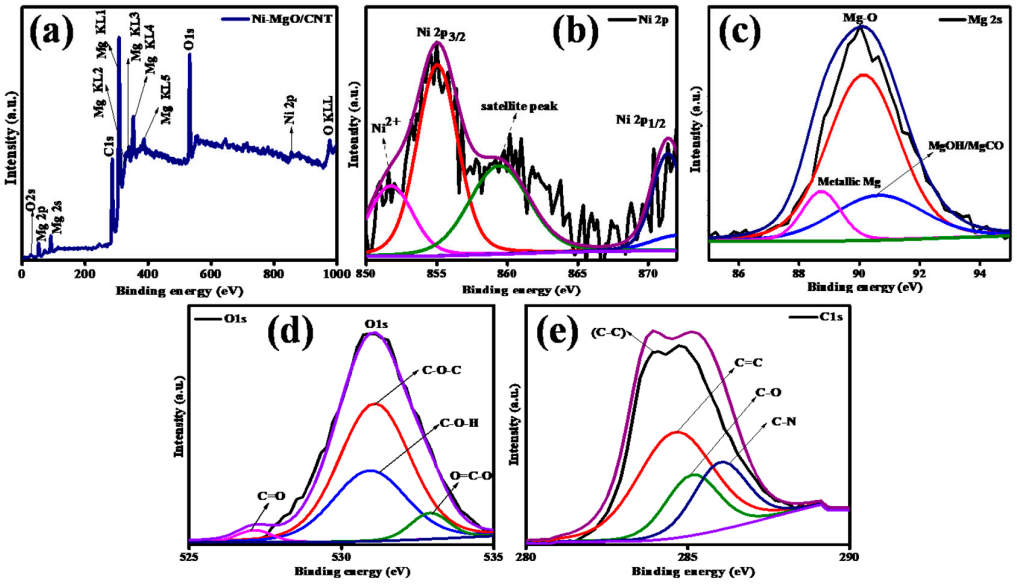

Figure 5. (a-e) XPS spectra of Ni-MgO /CNT; (a) overall survey spectra, (b) Ni2p, (c) Mg2s, (d) O1s and (e) C1s.

Preprints (www.preprints.org) | NOT PEER-REVIEWED | Posted: 26 December 2023 doi:10.20944/preprints202312.1992.v1

3.3. Electrocatalytic hydrogen evolution reaction

The HER were analyzed in three electrodes consisting of working (active material), reference (Ag/AgCl), counter (graphite rod) using 1 M alkaline KOH electrolyte solution in an ambient environment. All the applied potentials taken for the electrochemical analysis was converted to RHE along with standard Nernst reaction, $E_{RHE} = E_{Ag/AgCl} + E^{\circ}_{Ag/AgCl} + (0.059 \times pH)$. The cyclic voltammetry curves of the prepared pure MgO, MgO/CNT and Ni-MgO/CNT were studied from 0.9 to 1.0 (V) Vs RHE varying from 10 to 100 mV/s (Figure 6a-c). The attained CV exhibited ideal electrochemical double layer capacitance (EDLC) behavior and maintain good charge storage. Further, double layer capacitance (C_{dl}) values were evaluated by using the formula of $|j_a-j_c|/2\nu$, where $|j_a-j_c|$ represents the difference between anodic and cathodic current density and ν denotes the applied scan rates (mV/s). Additionally, ECSA values were estimated by applying $ECSA=C_{dl}/C_s$, which is depicted in the Figure 6(d). The optimized Ni-MgO/CNT electrocatalyst achieves the large C_{dl} and ECSA value of 20.6 mF cm^{-2} and 515 cm^2, respectively which is higher than those (5 mF cm^{-2} and 125 cm^2) of pure MgO and the values (17.2 mF cm^{-2} and 430 cm^2) of MgO/CNT. The large electrochemical surface area of Ni-MgO/CNT appears to be responsible for creating a large reactive active sites and escalating the possibility of subsequent charge ion transport [44].

The linear sweep voltammetry comparison of the prepared pure MgO, MgO/CNT and Ni-MgO/CNT catalysts at 2 mV/s was explored and presented in Figure 7(a). Among all other samples, Ni-MgO/CNT nanocomposite explored lowest 117 mV at 10 mA/cm^2, whereas the pure MgO and MgO/CNT exhibited the highest overpotential values of 147 mV and 141 mV, respectively. This suggests that incorporating Ni as a host element into MgO/CNT greatly improves the charge transfer efficiency and lowers the activation energy barrier to achieve an enhanced HER catalytic reaction. The enhanced electrochemical performance of the fabricated Ni-MgO/CNT electrocatalyst was compared with those reported in the earlier literature [45–52]. It will help to analyze the novel and integrated level of the electrocatalytic activity. For instance, the attained overpotential values were compared with previous literature as expressed in Table 1.

Table 1. Comparison of overpotential with previous literature works.

Catalyst	Electrolyte	j (mA/cm²)	η (mV)	Ref
Ni-N-C-250/Pt	KOH	10	400	45
Ni/$NiFe_2O_4$@PPy	KOH	10	127	46
Ni-Cu-Ti/CNTs-Ni	KOH	100	140	47
Ni/0.1$CePO_4$ catalyst	KOH	10	120	48
Ni-MSACs	KOH	10	270	49
NS-Ni/Mo_2C@NF	KOH	100	151	50
Ni_3S_2@NiS-250/NF	KOH	10	129	51
CNS/PHS/CP	KOH	10	186	52
Ni-MgO/CNT	KOH	10	117	Present study

Additionally, the intrinsic catalytic kinetics of the prepared samples as rate-limiting steps were evaluated by Tafel slope analysis using; $\eta=b \log(j) + a$ where η denoted as overpotential and j - current density, b denoted as Tafel slope which is shown in Figure 7b). Accordingly, the Ni-MgO/CNT nanocomposite electrocatalyst achieved 116 mV/dec Tafel value, smaller than pure MgO (133 mV/dec) and MgO/CNT (124 mV/dec). The hydrogen evolution reaction is semi half reactions of electrochemical water splitting which involves into two step electron transfer process. Initially, the molecular hydrogen from water was generated via HER by three different reaction pathways named as Volmer, Heyrovsky and Tafel. In an alkaline medium, primarily the adsorbed hydrogen intermediates (H_{ads}) were formed by the hydrolysis of the water molecule ($H_2O + e^- + \text{catalyst} \rightarrow \text{catalyst-}H_{ads} + OH^-$) which will mention as Volmer step (discharging). Also, the adsorbed hydrogen unites with the H^+ and e^- to form H_2 which is known as Heyrovsky step (desorption). The two adsorbed hydrogen on catalyst surface combine to form H_2 molecule acknowledged as Tafel step (chemical desorption step) [53]. Hence, the achieved Tafel value of 116 mV/dec is lower than the

 doi:10.20944/preprints202312.1992.v1

Volmer step (120 mV/dec), indicating the optimized electrode has good agreement with Volmer-Heyrovsky step of reaction mechanism of hydrogen absorption process (M-H_{ads}) occurred on electrode surface, which can increase charge transfer rate of Ni-MgO/CNT electrocatalyst [54].

Figure 7(c) shows the Nyquist plot of the as-prepared MgO, MgO/CNT and Ni-MgO/CNT samples. Comparatively, the Ni-MgO/CNT electrode exposed lower solution and charge transfer resistance compared to MgO/CNT and MgO electrodes because of the inverse correlation of charge transfer reaction kinetics and minimum charge transfer resistance of Ni-MgO/CNT electrode that is obviously seen in the Nyquist plot with the clear evidence of reduced arc. The electrochemical impedance (EIS) of Ni-MgO/CNT electrocatalyst was fitted with the corresponding equivalent circuit using Nyquist plots (Figure 7c). The semicircle in low frequency illustrated electrode charge transfer resistance (R_{ct}), Ni-MgO/CNT attained low R_{ct} value of 1.5 Ω and solution resistance (R_s) value of 0.75 Ω which is comparatively lower than all other electrodes of Pure MgO and MgO/CNT [55].

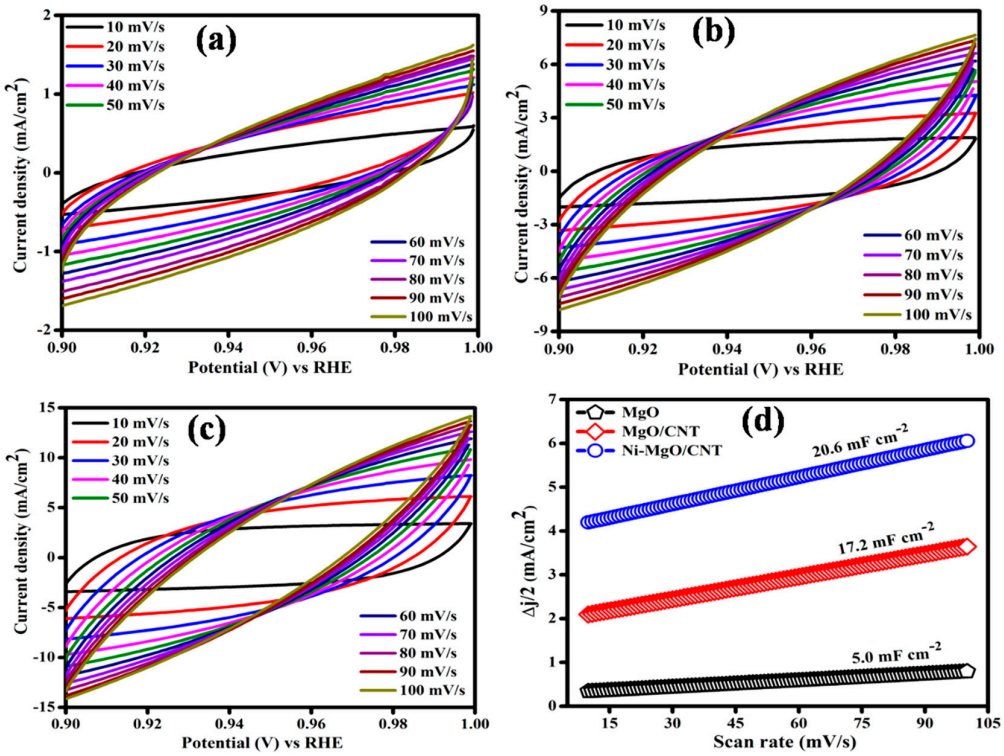

Figure 6. (a-c) CV curves, (d) ECSA linear plot of the prepared MgO, MgO/CNT and Ni-MgO/CNT nanocomposite.

Preprints (www.preprints.org) | NOT PEER-REVIEWED | Posted: 26 December 2023 doi:10.20944/preprints202312.1992.v1

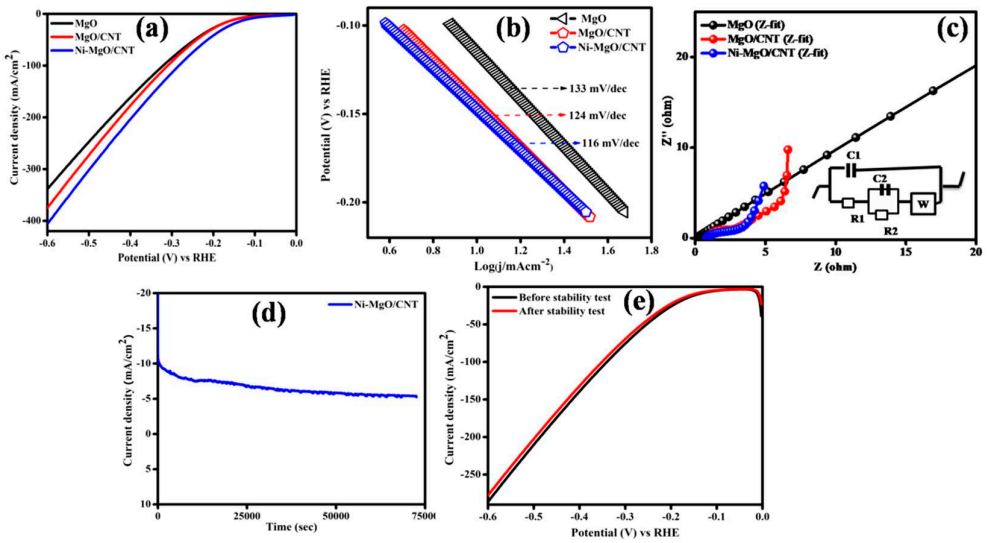

Figure 7. (a) LSV curve, (b) Tafel plot, (c) EIS (fitted) analysis, (d) chronoamperometry (CA) test and (e) LSV analysis after CA for the prepared MgO, MgO/CNT and Ni-MgO/CNT.

The durability and stability of fabricated electrode was systematically accessed via chronoamperometry testing, where starting potential was set at 10 mA/cm². The insightful results are illustrated in Figure 7(d), showcasing the electrode's commendable durability. Notably, the electrode exhibited robust stability, retaining 72% of its performance over a prolonged duration of 20 hours. While a slight decline in current density was observed, this change is further corroborated in the Linear Sweep Voltammetry (LSV) curve after stabilization, depicted in Figure 7(e) [56]. This observed stability positions the Ni-MgO/CNT composite as an optimal electrocatalyst for enduring energy applications. The minimal degradation over an extended period, coupled with the slight decline in current density, show up its reliability and suitability for sustained electrocatalytic activity. These findings highlight the Ni-MgO/CNT potential for long-term energy applications, attributing its performance to a high thermal capacity within alkaline media.

4. Conclusions

Ni-MgO/CNT nanocomposites with the improved specific surface area were synthesized through the cost-effective impregnation and chemical vapor deposition methods. The comparison of the peaks from Ni-MgO/CNT to those from MgO/CNT revealed no major differences except the broad and low intensity peak at 2θ = 44.2º in Ni-MgO/CNT. The broad and low intense diffraction peak centered at around 44~45º are known to belong to the amorphous Ni. The G-band to D-band relative intensity ratio observed in Raman is greater in Ni-MgO/CNT, indicating more defects in the synthesized Ni-MgO/CNT compared to those in MgO/CNT. The presence of G' band in Raman spectra supports the higher fraction of CNTs in Ni-MgO/CNT than in MgO/CNT (green), although more defects were introduced in CNT of Ni-MgO/CNT because of its faster growth facilitated by the catalytic function of Ni. The evaluation of morphological features of Ni-MgO/CNT nanocomposites revealed the presence of helical-shaped CNTs adorning the surface of Ni-MgO flakes with the growth of CNTs facilitated by the catalytic activity of Ni. The abundance of CNTs in Ni-MgO/CNT compared to those in MgO/CNT supports the faster growth facilitated by the catalytic action. Notably, the electrochemical performance of Ni-MgO/CNT demonstrated remarkably low 117 mV at 10 mA cm^{-2} signifying exceptional catalytic activity toward hydrogen evolution reaction (HER). The explored high electrochemical surface area (ECSA) value of 515 cm² and low charge transfer resistance of 1.5 Ω are indicative of enhanced active metal sites and efficient ion transportation during the electrode-electrolyte interaction. Notably, the processed electrode in the present study exhibited robust stability, retaining 72% of its performance over a prolonged duration of 20 hours. While a slight

decline in current density was observed, this change is further corroborated in the Linear Sweep Voltammetry (LSV) curve after stabilization. The observed stability positions of the Ni-MgO/CNT composite is as an optimal electrocatalyst for enduring energy applications. The commendable catalytic action and the enhanced stability of the synthesized electrodes suggests the potential reusability of the Ni-MgO/CNT electrode for diverse applications.

Author Contributions: "Conceptualization, P. M.. R. Y.; methodology, M. I., J.H.H.; investigation, P. M, L. K.; formal analysis, S. A., P/M., ; resources, G. R.; data curation, J.H.H. M. L.; writing—original draft preparation, S.I.H., R. Y.; review and editing, S.I.H., R. Y.; supervision, R. Y. All authors have read and agreed to the published version of the manuscript.".

Funding: This work was supported by UGC-SAP, DST-FIST, DST-PURSE and RUSA grants in India and also by the National Research Foundation of Korea (NRF) grant (No. 2021R1A4A1031494) in Korea.

Data Availability Statement: Data will available on request.

Conflicts of Interest: Declare conflicts of interest or state "The authors declare no conflicts of interest.".

References

1. Wang, M.; Wang, Z.; Gong, X.; Guo, Z. The intensification technologies to water electrolysis for hydrogen production–A review. *Renewable and sustainable energy reviews*, **2014**, *29*, pp.573-588.
2. Züttel, A.; Remhof, A.; Borgschulte, A.; Friedrichs, O. Hydrogen: the future energy carrier. *Philosophical Transactions of the Royal Society A: Mathematical, Physical and Engineering Sciences*, **2010**, *368*(1923), pp.3329-3342.
3. Susmozas, A.; Iribarren, D.; Dufour, J. Life-cycle performance of indirect biomass gasification as a green alternative to steam methane reforming for hydrogen production. *International Journal of hydrogen energy*, **2013**, *38*(24), pp.9961-9972.
4. Zou, X.; Zhang, Y. Noble metal-free hydrogen evolution catalysts for water splitting. *Chemical Society Reviews*, **2015**, *44*(15), pp.5148-5180.
5. Li, X.; Hao, X.; Abudula, A.; Guan, G. Nanostructured catalysts for electrochemical water splitting: current state and prospects. *Journal of Materials Chemistry A*, **2016**, *4*(31), pp.11973-12000.
6. Son, M.-K. Key strategies on Cu_2O photocathodes toward practical photoelectrochemical water splitting, *Nanomaterials*, **2023**, 13, 3142.
7. Yoon, S. J.; Lee, S. J.; Kim, M. H.; Park, H. A.; Kang, H. S.; Bae, S-Y.; Jeon, I-Y. Recent Tendency on Transition-Metal Phosphide Electrocatalysts for the Hydrogen Evolution Reaction in Alkaline Media, *Nanomaterials*, **2023**, 13, 2613.
8. Durst, J.; Siebel, A.; Simon, C.; Hasché, F.; Herranz, J.; Gasteiger, H.A. New insights into the electrochemical hydrogen oxidation and evolution reaction mechanism. *Energy & Environmental Science*, **2014**, *7*(7), pp.2255-2260.
9. Deng, J.; Ren, P.; Deng, D.; Yu, L.; Yang, F.; Bao, X. Highly active and durable non-precious-metal catalysts encapsulated in carbon nanotubes for hydrogen evolution reaction. *Energy & Environmental Science*, **2014**, *7*(6), pp.1919-1923.
10. Yu, F.; Yu, L.; Mishra, I.K.; Yu, Y.; Ren, Z.F.; Zhou, H.Q. Recent developments in earth-abundant and non-noble electrocatalysts for water electrolysis. *Materials Today Physics*, **2018**, *7*, pp.121-138.
11. Sun, H.; Yan, Z.; Liu, F.; Xu, W.; Cheng, F.; Chen, J. Self-supported transition-metal-based electrocatalysts for hydrogen and oxygen evolution. *Advanced materials*, **2020**, *32*(3), p.1806326.
12. Yuan, S.; Duan, X.; Liu, J.; Ye, Y.; Lv, F.; Liu, T.; Wang, Q.; Zhang, X. Recent progress on transition metal oxides as advanced materials for energy conversion and storage. *Energy Storage Materials*, **2021**, *42*, pp.317-369.
13. Pilarska, A.A.; Klapiszewski, L.; Jesionowski, T. Recent development in the synthesis, modification and application of $Mg(OH)_2$ and MgO: A review. *Powder Technology*, **2017**, *319*, pp.373-407.
14. Abdulaziz, A. M.A.; Ahmed, S. A.F.; Naitik, P.; Salwa, B. A.; Nouf, A. B.; Ahmed, A. I.; Ahmed, Y. El.; Jehad, K. A.; Ahmed, E. A.; Anis, H. F.; Rawesh, K. Alumina-Magnesia-Supported Ni for Hydrogen Production via the Dry Reforming of Methane: A Cost-Effective Catalyst System, *Nanomaterials*, **2023**, 13, 2984.
15. Yuan, C.; Wu, H.B.; Xie, Y.; Lou, X.W. Mixed transition-metal oxides: design, synthesis, and energy-related applications. *AngewandteChemie International Edition*, **2014**, *53*(6), pp.1488-1504.
16. Zhang, Q.; Huang, J.Q.; Qian, W.Z.; Zhang, Y.Y.; Wei, F. The road for nanomaterials industry: A review of carbon nanotube production, post-treatment, and bulk applications for composites and energy storage. *Small*, **2013**, *9*(8), pp.1237-1265.

17. Peng, L.; Zheng, X.; Li, L.; Zhang, L.; Yang, N.; Xiong, K.; Chen, H.; Li, J.; Wei, Z. Chimney effect of the interface in metal oxide/metal composite catalysts on the hydrogen evolution reaction. *Applied Catalysis B: Environmental*, **2019**, *245*, pp.122-129.
18. Liu, W.; Tan, W.; He, H.; Yang, Y. Electrodeposition of self–supported Ni–Mg–La electrocatalyst on Ni foam for efficient hydrogen evolution reaction. *ElectrochimicaActa*, **2022**, *411*, p.140058.
19. Darband, G.B.; Aliofkhazraei, M.; Rouhaghdam, A.S. Three-dimensional porous Ni-CNT composite nanocones as high performance electrocatalysts for hydrogen evolution reaction. *Journal of Electroanalytical Chemistry*, **2018**, *829*, pp.194-207.
20. Qazi, U.Y.; Javaid, R.; Tahir, N.; Jamil, A.; Afzal, A. Design of advanced self-supported electrode by surface modification of copper foam with transition metals for efficient hydrogen evolution reaction. *International Journal of Hydrogen Energy*, **2020**, *45*(58), pp.33396-33406.
21. Zhu, S.; Zhao, N.; Li, J.; Deng, X.; Sha, J.; He, C. Hard-template synthesis of three-dimensional interconnected carbon networks: rational design, hybridization and energy-related applications. *Nano Today*, **2019**, *29*, p.100796.
22. Vaka, M.; Walvekar, R.; Yanamadala, S. Carbon nanotubes and their composites: from synthesis to applications. *Contemporary nanomaterials in material engineering applications*, **2021**, pp.37-67.
23. Jourdain, V.; Bichara, C. Current understanding of the growth of carbon nanotubes in catalytic chemical vapour deposition. *Carbon*, **2013**, *58*, pp.2-39.
24. Zhang, J.; Zhang, Z.; Ji, Y.; Yang, J.; Fan, K.; Ma, X.; Wang, C.; Shu, R; Chen, Y. Surface engineering induced hierarchical porous Ni12P5-Ni2P polymorphs catalyst for efficient wide pH hydrogen production. *Applied Catalysis B: Environmental*, **2021**, *282*, p.119609.
25. Rao, K.G.; Ashok, C.H.; Rao, K.V.; Chakra, C.S. Structural properties of MgO nanoparticles: synthesized by co-precipitation technique. *International Journal of Science and Research*, **2014**, *3*(12), pp.43-46.
26. Khachatur Manukyan, V.; Christopher Shuck, E.; Mathew Cherukara, J.; Sergei Rouvimov.; Dmitry Kovalev, Y.; Alejandro Strachan.; Alexander Mukasyan, S.; Exothermic Self-Sustained Waves with Amorphous Nickel. *J. Phys. Chem. C*, **2016**, 120, pp. 5827−5838
27. Abazari, S.; Shamsipur, A.; Bakhsheshi-Rad, H.R.; Keshavarz, M.; Kehtari, M.; Ramakrishna, S.; Berto, S. MgO-incorporated carbon nanotubes-reinforced Mg-based composites to improve mechanical, corrosion, and biological properties targeting biomedical applications. *Journal of Materials Research and Technology*, **2022**, 20, pp976~990.
28. Imran Ali.; Tahani Saad AlGarni.; Elena Burakova.; Alexey Tkachev.; Evgeny Tugolukov.; Tatyana Dyachkova.; Artem Rukhov.; Irina Gutnik.; Evgeny Galunin. A new approach to the economic synthesis of multi-walled carbon nanotubes using a Ni/MgO catalyst, *Materials Chemistry and Physics*, **2021**, 261. 124234.
29. Ghazaleh Allaedini.; Siti Masrinda Tasirin.; Payam Aminayi.; Synthesis of CNTs via chemical vapor deposition of carbon dioxide as a carbon source in the presence of NiMgO, *Journal of Alloys and Compounds*, **2015**, 647, pp809-814.
30. Ryu, H.; Singh, B.K.; Bartwal, K.S. Synthesis and optimization of MWCNTs on Co-Ni/MgO by thermal CVD, *Advances in condensed matter physics*, **2008**.
31. ZHANG, Q.; Yi, L.; Ling, H.U.; Qian, W.Z.; Luo, G.H.; Fei, W. Synthesis of thin-walled carbon nanotubes from methane by changing the Ni/Mo ratio in a Ni/Mo/MgOcatalyst, *New Carbon Materials*, **2008**, 23(4), pp.319-325.
32. Zhou, L.P.; Ohta, K.; Kuroda, K.; Matsuishi, K.; Gao, L.; Matsumoto, T.; Nakamura, J. Catalytic functions of Mo/Ni/MgO in the synthesis of thin carbon nanotubes, *The Journal of Physical Chemistry B*, **2005**, 109(10), pp.4439-4447.
33. Zhu, K., Hu, J., Kobel, C., and Richards, R. Efficient Preparation and Catalytic Activity of MgO(111) Nanosheets, Angew. Chem. Int. Ed. **2006**, 45, pp7277 –7281
34. Taleshi, F.; Hosseini, A.A. Synthesis of uniform MgO/CNT nanorods by precipitation method, *Journal of Nanostructure in Chemistry*, **2012**, 3, pp.1-5.
35. Ding, Y.D.; Song, G.; Zhu, X.; Chen, R.; Liao, Q. Synthesizing MgO with a high specific surface for carbon dioxide adsorption. *Rsc Advances*, **2015**, *5*(39), pp.30929-30935.
36. Allaedini, G.; Tasirin, S.M.; Aminayi, P. Synthesis of CNTs via chemical vapor deposition of carbon dioxide as a carbon source in the presence of NiMgO. *Journal of Alloys and Compounds*, **2015**, 647, pp.809-814.
37. Ikram, M.; Inayat, T.; Haider, A.; Ul-Hamid, A.; Haider, J.; Nabgan, W.; Saeed, A.; Shahbaz, A.; Hayat, S.; Ul-Ain, K.; Butt, A.R. Graphene oxide-doped MgO nanostructures for highly efficient dye degradation and bactericidal action. *Nanoscale research letters*, **2021**, *16*, pp.1-11.
38. Pant, N.; Yanagida, M.; Shirai, Y.; Miyano, K. Effect of different surface treatments of sputtered NiOX on the photovoltaic parameters of perovskite solar cells: a correlation study. *Applied physics express*, **2020**, *13*(2), p.025505.
39. Branca, C.; Frusteri, F.; Magazu, V.; Mangione, A. Characterization of carbon nanotubes by TEM and infrared spectroscopy. *The Journal of Physical Chemistry B*, **2004**, *108*(11), pp.3469-3473.

40. Le Febvrier, A.; Jensen, J.; Eklund, P. Wet-cleaning of MgO (001): Modification of surface chemistry and effects on thin film growth investigated by x-ray photoelectron spectroscopy and time-of-flight secondary ion mass spectroscopy. *Journal of Vacuum Science & Technology A*, **2017**, *35*(2), 021407.
41. Skorupska, M.; Kamedulski, P.; Lukaszewicz, J.P.; Ilnicka, A. The improvement of energy storage performance by sucrose-derived carbon foams via incorporating nitrogen atoms. *Nanomaterials*, **2021**, *11*(3), p.760.
42. Yumitori, S. Correlation of C1s chemical state intensities with the O1s intensity in the XPS analysis of anodically oxidized glass-like carbon samples. *Journal of materials science*, **2000**, *35*, pp.139-146.
43. Dwivedi, N.; Yeo, R.J.; Satyanarayana, N.; Kundu, S.; Tripathy, S.; Bhatia, C.S. Understanding the role of nitrogen in plasma-assisted surface modification of magnetic recording media with and without ultrathin carbon overcoats. *Scientific reports*, **2015**, *5*(1), p.7772.
44. Peng, Y.; Lu, B.; Chen, S. Carbon-supported single atom catalysts for electrochemical energy conversion and storage. *Advanced Materials*, **2018**, *30*(48), p.1801995.
45. Wang, Q.; Hou, M.; Huang, Y.; Li, J.; Zhou, X.; Ma, G.; Ren, S. One-pot synthesis of NiCoP/CNTs composites for lithium ion batteries and hydrogen evolution reaction. *Ionics*, **2020**, *26*, pp.1771-1778.
46. Li, P.; Zhao, G.; Cui, P.; Cheng, N.; Lao, M.; Xu, X.; Dou, S.X.; Sun, W. Nickel single atom-decorated carbon nanosheets as multifunctional electrocatalyst supports toward efficient alkaline hydrogen evolution. *Nano Energy*, **2021**, *83*, p.105850.
47. Jia, L.; Du, G.; Han, D.; Wang, Y.; Zhao, W.; Su, Q.; Ding, S.; Xu, B. Magnetic electrode configuration with polypyrrole-wrapped Ni/NiFe2O4 core–shell nanospheres to boost electrocatalytic water splitting. *Chemical Engineering Journal*, **2023**, *454*, p.140278'
48. Wu, L.; Ji, L.; Wang, H.; Li, X.; Wu, X.; Zeng, S.; Li, L.; Xiao, Y.; Zhang, Q. Preparation and hydrogen evolution performance of porous Ni-Cu-Ti/CNTs-Ni electrode. *Vacuum*, **2023**, *218*, p.112598.
49. Ke, H.; Wang, J.; Yu, N.; Pu, Y.; Tan, J.; Gong, M.; Zhang, W.; Xue, Y.; Yu, F. Interface-engineered Ni/CePO4 heterostuctures for efficient electro-/photo-catalytic hydrogen evolution. *Fuel*, **2023**, *344*, p.127971.
50. Park, J.W.; Park, G.; Kim, M.; Han, M.; Jang, J.; Yamauchi, Y.; Yuliarto, B.; Krüger, P.; Kim, J.; Park, N.; Lim, H. Ni-single atom decorated mesoporous carbon electrocatalysts for hydrogen evolution reaction. *Chemical Engineering Journal*, **2023**, *468*, p.143733.
51. Liu, Z.; He, H.; Liu, Y.; Zhang, Y.; Shi, J.; Xiong, J.; Zhou, S.; Li, J.; Fan, L.; Cai, W. Soft-template derived Ni/Mo2C hetero-sheet arrays for large current density hydrogen evolution reaction. *Journal of Colloid and Interface Science*, **2023**, *635*, pp.23-31.
52. Chen, M.; Su, Q.; Kitiphatpiboon, N.; Zhang, J.; Feng, C.; Li, S.; Zhao, Q.; Abudula, A.; Ma, Y.; Guan, G. Heterojunction engineering of Ni3S2/NiS nanowire for electrochemical hydrogen evolution. *Fuel*, **2023**, *331*, p.125794.
53. Lasia, A. Mechanism and kinetics of the hydrogen evolution reaction. *international journal of hydrogen energy*, **2019**, *44*(36), pp.19484-19518.
54. Li, X.; Yan, W.; Fan, B.; Wang, Z. Lattice-controllable in-situ synthesis of Co-Ni-mixed sulfide/polypyrrole nanostructures on carbon paper for hydrogen evolution reaction in alkaline media. *Journal of Alloys and Compounds*, **2023**, *960*, p.170730.
55. Gong, M.; Zhou, W.; Tsai, M.C.; Zhou, J.; Guan, M.; Lin, M.C.; Zhang, B.; Hu, Y.; Wang, D.Y.; Yang, J.; Pennycook, S.J. Nanoscale nickel oxide/nickel heterostructures for active hydrogen evolution electrocatalysis. *Nature communications*, **2014**, *5*(1), p.4695.
56. Bredar, A.R.; Chown, A.L.; Burton, A.R.; Farnum, B.H. Electrochemical impedance spectroscopy of metal oxide electrodes for energy applications. *ACS Applied Energy Materials*, **2020**, *3*(1), pp.66-98.